ELSEVIER

Surface Science 410 (1998) 270–282

surface science

Adsorption of oxygen on Au(111) by exposure to ozone

N. Saliba [a], D.H. Parker [b], B.E. Koel [a,*]

[a] *Department of Chemistry, University of Southern California, Los Angeles, CA 90089-0482, USA*
[b] *Dow Chemical Company, 1897 Building, Midland, MI 48667, USA*

Received 2 September 1997; accepted for publication 17 March 1998

Abstract

Atomic oxygen coverages of up to 1.2 ML may be cleanly adsorbed on the Au(111) surface by exposure to O_3 at 300 K. We have studied the adsorbed oxygen layer by AES, XPS, HREELS, LEED, work function measurements and TPD. A plot of the O(519 eV)/Au(239 eV) AES ratio versus coverage is nearly linear, but a small change in slope occurs at $H_0 = 0.9$ ML. LEED observations show no ordered superlattice for the oxygen overlayer for any coverage studied. One-dimensional ordering of the adlayer occurs at low coverages, and disordering of the substrate occurs at higher coverages. Adsorption of 1.0 ML of oxygen on Au(111) increases the work function by +0.80 eV, indicating electron transfer from the Au substrate into an oxygen adlayer. The O(1s) peak in XPS has a binding energy of 530.1 eV, showing only a small (0.3 eV) shift to a higher binding energy with increasing oxygen coverage. No shift was detected for the Au $4f_{7/2}$ peak due to adsorption. All oxygen is removed by thermal desorption of O_2 to leave a clean Au(111) surface after heating to 600 K. TPD spectra initially show an O_2 desorption peak at 520 K at low H_0, and the peak shifts to higher temperatures for increasing oxygen coverages up to $H_0 = 0.22$ ML. Above this coverage, the peak shifts very slightly to higher temperatures, resulting in a peak at 550 K at $H_0 = 1.2$ ML. Analysis of the TPD data indicates that the desorption of O_2 from Au(111) can be described by first-order kinetics with an activation energy for O_2 desorption of 30 kcal mol^{-1} near saturation coverage. We estimate a value for the Au–O bond dissociation energy D(Au–O) to be ~56 kcal mol^{-1}.

Keywords: Adatoms; Adsorption kinetics; Auger electron spectroscopy (AES); Chemisorption; Compound formation; Gold; Low energy electron diffraction (LEED); Low index single crystal surfaces; Oxidation; Oxygen; Ozone; Soft X-ray photoelectron spectroscopy; Thermal desorption

1. Introduction

Compared to the other metals, gold is the noblest of all metals and has little activity for chemisorption [1]. However, the interesting catalytic properties of gold warrant further fundamental study. A review article by Schwank [2] detailed many of the earlier applications of elemental gold in catalysis, including its high selectivity for olefin hydrogenation, hydrogen transfer reactions, and skeletal isomerizations of hydrocarbons, the striking activities for oxygen transfer reactions, the reduction of nitric oxide and the carbonyl group in acetone, and the oxidative dehydrogenation of alcohols to aldehydes. More recently, a lot of attention has been focused on the use of gold supported on reducible metal oxides as highly active, low-temperature CO oxidation catalysts [3–19]. Further elucidation of the role of oxygen in these reactions requires a better understanding of the interactions of oxygen with gold surfaces.

* Corresponding author. Fax: +1 213 740 3972; e-mail: koel@chem1.usc.edu

0039-6028/98/$19.00
PII: S0039-6028(98)00309-4

Early work on the interaction of oxygen with gold surfaces was often contradictory. Chesters and Somorjai [20] studied the chemisorption of O_2 on Au(111) and stepped Au surfaces and found oxygen chemisorption to be highly exothermic, but rapid only above 500°C. The presence of steps did not influence this behavior. Schrader [21] found that surface-segregated calcium can strongly increase the rate of O_2 chemisorption above 600°C. Eley and Moore [22] found that very little oxygen could be chemisorbed on polycrystalline Au foil for temperatures less than 1000 K and O_2 pressures less than 6×10^{-3} Pa. Legaré et al. [23] studied the interaction of O_2 with Au(111) and polycrystalline Au foil over a wide range of temperatures ($25<T<850$°C) and pressures ($10^{-8}<P<10$ Torr) and found that no oxygen could be adsorbed at 25°C for all O_2 pressures studied. However, oxygen could be adsorbed on both surfaces at temperatures above 300°C, and calcium was found to increase the amount of oxygen adsorbed. These contradictions in the early studies were explained by Pireaux et al. [24], who determined that O_2 does not dissociatively adsorb on gold surfaces in UHV, except when an impurity is present. The impurity level required for the adsorption of O_2 is below the level of detection by AES due to gold transitions that interfere with the detection of the most common contaminants (Ca, Mg, and Si). HREELS was used by Pireaux et al. [24], and this has sufficient sensitivity to observe the oxide impurities formed by exposure of O_2 to a contaminated surface. Canning et al. also [25] confirmed that no oxygen adsorption on clean gold occurred from exposure to O_2 in UHV, but studied adsorbed oxygen by dissociating O_2 over a hot Pt filament in order to expose the surface to oxygen atoms. The use of oxygen d.c. reactive sputtering to form a stable gold oxide, Au_2O_3, was also reported by Pireaux et al. [26].

About 10 years ago, on the Au(110)-(1×2) surface, Sault et al. [27] used O_2 pressures up to 1400 Torr and temperatures between 300 and 500 K, and did not observe any dissociative O_2 adsorption. Coverages of 0.95 ML of atomically adsorbed oxygen could be formed by O_2 dissociation over a hot filament, and recombinative desorption occurred at 590 K with an activation energy of 31.5 kcal mol^{-1}. On Au(111), no oxygen adsorption was detected after O_2 exposures, but near monolayer coverages of atomically adsorbed oxygen were also created under UHV conditions by dosing ozone (O_3) to the surface at 300 K [28,29]. Thermal desorption of O_2 occurred at 560 K at saturation coverage with an activation energy of 30 kcal mol^{-1}. UV/ozone oxidation of gold under UHV conditions leads to more extensive oxidation [30,31]. It was estimated by using XPS data that this treatment formed 0.8 ML of chemisorbed oxygen along with a few monolayers of Au_2O_3 upon extensive oxidation of (111) textured Au films [30]. Both oxygen states disappeared when heated to 150–200°C [30]. This is reasonably consistent with the reported decomposition temperature of 423 K for bulk Au_2O_3 [32].

Some conflicting reports still surface. Cao et al. [33] reported that a chemisorbed state of oxygen on Au(111) was formed after O_2 exposures at a pressure of 5×10^{-6} mbar and a temperature ranging from 600 to 850°C, that this state could not be removed by heating up to 850°C in vacuum, and that a twisted oxide (AuO_x) overlayer and (3×3)R30° structure with further oxygen adsorption was formed. Recent STM studies [34–36] reproduced the (3×3)R30° overlayer structure on Au(111), not under UHV conditions, but only after an O_2 pressure of 1 bar and temperatures between 500 and 800°C were used. Still, these authors assigned this structure to strongly chemisorbed oxygen.

In this paper, we report additional studies of the interaction of oxygen on a Au(111) crystal surface by using ozone (O_3) to cleanly dose the surface with atomic oxygen. The chemical nature of the oxygen adlayer on Au(111) was characterized by a variety of surface spectroscopies, and the thermal stability of the oxygen adlayer was probed by TPD in order to provide a foundation for understanding low-temperature oxidation over supported Au catalysts and to clarify issues raised in some recent surface science reports.

2. Experimental

The experiments were performed in a two-level stainless steel UHV chamber which has been described previously [37]. The system was equ-

ipped with the instrumentation necessary to perform AES, LEED, XPS, UPS, HREELS and TPD. The Au(111) crystal was heated resistively and cooled by contact of the crystal mounting block with a liquid nitrogen reservoir through a 6.45 cm^2 (1 in^2), 0.025 cm thick (0.01 in) sapphire plate. The temperature of the Au(111) crystal was monitored directly by means of a chromel–alumel thermocouple pressed firmly (using Au foil) into a small hole drilled into the side of the crystal.

The Au(111) crystal was cleaned by heating in 2×10^{-8} Torr of NO_2 at 800 K to remove carbon from the surface. Oxygen was detected by AES after this procedure, even after heating to 1000 K. Oxygen that is stable at such high temperatures on gold is known to be due to oxides of calcium and/or silicon, yet these impurities were not detected by AES, even after extended heating to high temperatures. This oxide was removed by argon ion sputtering at 800 K. Cycles of cleaning in NO_2 followed by argon ion sputtering were repeated until the oxide could no longer be formed by NO_2 exposure and carbon was no longer detected. The crystal was then annealed to 800 K and gave the expected LEED pattern for the reconstructed surface [38,39].

Ozone (O_3) used for dosing was prepared in our laboratory using a commercial ozone generator and concentrated on a silica gel trap. Oxygen (O_3) was passed at a rate of 5 ml min^{-1} (STP) through Teflon tubing to the ozone generator. The effluent gas from the generator contained a mixture of approximately 5% ozone and 95% unreacted O_2. This mixture was passed through a gas absorption bottle containing dried silica gel suspended in a dewar filled with an ethanol–dry ice bath at -80°C. This process was carried out for several hours to saturate the silica gel with ozone. The ozone may be kept indefinitely at -80°C, but we warn users that there is always a chance of explosion if it is allowed to warm up or accidentally come into contact with the ethanol in the bath. Since a great deal of O_2 is usually present as an impurity, the ozone was purified by cooling the trap to -110°C and pumping out the O_2 with a mechanical pump. The trap was then allowed to warm up to -80°C. Because ozone is such a reactive molecule, it was necessary to rigorously passivate the stainless steel gas handling line and any copper components (e.g. gaskets) by flushing the lines several times with ozone. We found that ozone still decomposed in the lines over a period of minutes, and therefore, it was necessary to recharge the lines frequently. A glass microcapillary array doser was connected to the leak valve on the chamber and was used for dosing ozone directly on to the sample. All ozone dosing was performed with the Au(111) crystal at 300 K.

TPD experiments were performed with the quadrupole mass spectrometer in line-of-sight with the crystal. The heating rate was 8.5 K s^{-1}. Signals at 16, 18, 32, and 48 amu were monitored initially to detect desorption of any water impurity, oxygen, and ozone. Water was only detected when the crystal was allowed to stand at 100 K for extended periods of time. No molecular desorption of ozone was observed in these experiments.

AES spectra were recorded using an incident beam energy of 3 keV and a 0.2 mA emission-regulated beam current with a modulation voltage of 6 V_{p-p}. Work function measurements ($D\Phi$) were made by measuring the onset of secondary electron emission in UPS. XPS binding energies (BE) are referred to the Au $4f_{7/2}$ peak at 84.0 eV BE for clean Au(111).

3. Results and discussion

3.1. AES and oxygen coverage

Fig. 1 shows the AES peak-to-peak height ratio of the O(KLL) 519 eV signal to the Au(MNN) 239 eV signal plotted as a function of oxygen coverage. The relative oxygen coverage was determined by integration of O_2 TPD curves to determine the peak areas. The absolute oxygen coverage was estimated by comparing the O(519 eV)/Au(239 eV) AES peak-to-peak height ratio with the O(519 eV)/Pt(237 eV) ratio that was obtained in the same instrument for the (2×2)-O adlayer on Pt(111) where the oxygen coverage has been determined to be 0.25 ML or 3.8×10^{14} atoms cm^{-2} [40]. In this determination, we accounted for the reported difference in sensitivi-

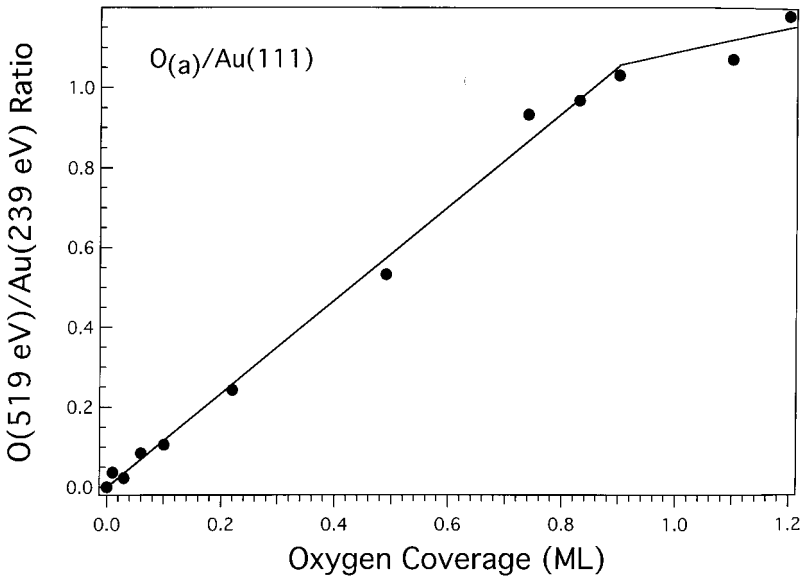

Fig. 1. Peak-to-peak height ratio for O(519 eV)/Au(239 eV) in AES for increasing oxygen coverage as determined from O_2 TPD integrated areas, on Au(111) at 300 K.

ties between Pt (237 eV) (0.028) and Au(239 eV) (0.037) transitions [41] and calibrated the two ratios at a low oxygen coverage of 0.25 ML where we believe that all of the oxygen is adsorbed on the Au(111) surface (vide infra). We estimate that the saturation coverage of oxygen that we obtained using O_3 and our dosing procedure on Au(111) was $H_0 = 1.2$ ML. Obvious uncertainties in the above calibration procedure, e.g. Auger lineshape changes, coadsorbates, etc., probably force error bars on our values for H_0 on Au(111) to be ± 0.1 ML.

The plot in Fig. 1 shows a noticeable change in slope near $H_0 = 0.9$ ML. Since the O(519 eV) signal arises from a KVV transition, the oxygen line shape and intensity are sensitive to changes in the chemical nature of the oxygen, and this could possibly cause this change. Alternatively, the slope change can be attributed to intensity changes (due to scattering) of either the oxygen or Au signals that result from the disordering of the Au(111) substrate, as seen in LEED at this oxygen coverage (vide infra), or to incorporation of oxygen into the surface or subsurface layer to form an oxide.

3.2. LEED observations

LEED photographs obtained as a function of oxygen coverage are shown in Fig. 2. The clean Au(111) surface is known to reconstruct in UHV to a (3×22)-rect. pattern in which each integral order spot is closely surrounded by a hexagonal cluster of six spots [38,39]. Fig. 2A shows the clean surface with the integral order spots surrounded by a poorly resolved cluster of the extra spots expected for the reconstructed surface. A small amount ($H_0 < 0.1$ ML) of adsorbed oxygen lifts this reconstruction and leaves only the sharp integral order spots. At higher coverages, as shown in Fig. 2B and C for $H_0 = 0.22$ ML and 0.50 ML, respectively, streaks appear that radiate between each of the integral order spots, appearing brightest halfway between the integral order spots. This pattern persists with increased intensity of the background until saturation oxygen coverage is reached, at which point the background is so bright that the substrate spots are almost obscured (Fig. 2D). The streaking indicates the onset of one-dimensional ordering. The brightness of the

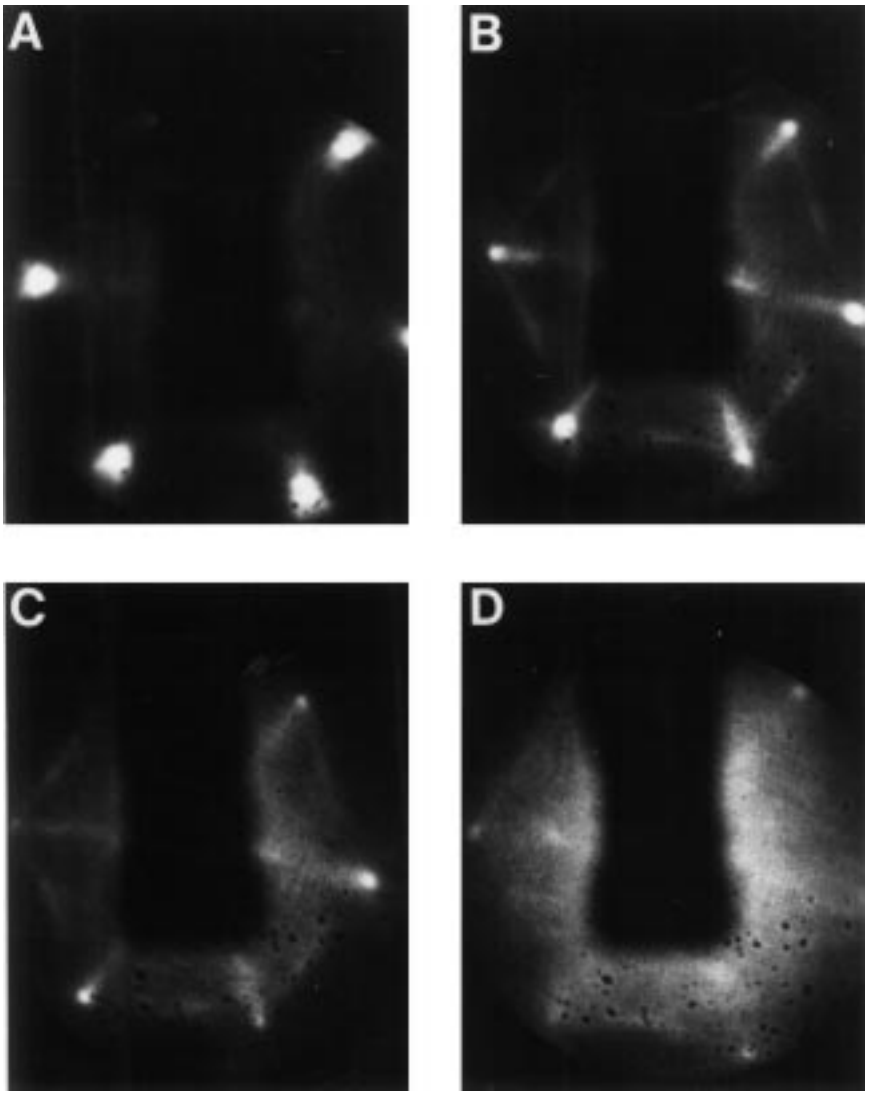

Fig. 2. LEED photographs taken at several oxygen coverages using an incident beam energy of ~66 eV. (A) Clean Au(111), (B) 0.22 ML, (C) 0.5 ML and (D) 1.2 ML.

background at saturation oxygen coverage indicates disordering of the substrate itself with significant displacement of the gold atoms.

Our LEED results are quite similar to those reported by Sault et al. [27] for oxygen on Au(110)-(1×2). Using a hot mass spectrometer filament to produce O atoms, they also saw a large increase in background intensity due to a disruption of the long-range order of the surface, but did not observe any ordered overlayer patterns at any coverage or annealing temperature. The streaking that we observed is consistent with the row-like features seen in STM studies of the Au(111) surface after high-temperature O_2 exposures at high pressure [34–36]. However, since we did not observe a $(3\times3)R30^\circ$ LEED pattern, our results contradict those reported by Cao et al. [33] in which they exposed O_2 on Au(111) at 600°C in vacuum, and are inconsistent with a $(3\times3)R30^\circ$ structure ascribed to chemisorbed oxygen [34,35].

3.3. Work function measurements

Fig. 3 shows the work function change (Dw) as a function of oxygen coverage. The sign of Dw indicates electron transfer from the gold into an adsorbed oxygen overlayer. The work function change (eV) with coverage data can be treated by a classical model for mobile adsorption:

$$Dw = \frac{3.77 \times 10^{-15} H m}{1 + 9 a H 3/2}, \quad (1)$$

where H is the surface oxygen coverage (atoms cm^{-2}), m is the dipole moment (*D*), and a is the polarizability (cm^3) [42,43]. The solid curve in Fig. 3 was obtained using $m = 0.34D$ and $a = 2.46 \times 10^{-24}\ cm^3$ to give a reasonably good fit to our measured values. However, some of the deviations from this curve may be real and significant. For comparison, the O/Pt(111) system shows a linear behavior up to an oxygen coverage of 0.75 ML [40]. Why should Au(111) be so different? Alternatively, the data in Fig. 3 for $H_0 \leq 0.1$ ML may be viewed in terms of a relatively large Dw associated with lifting the reconstruction of the clean Au(111) surface (as observed in LEED), or possibly due to the population of defect sites, giving a larger value for m at these low coverages. Since the Helmholtz equation gives $m = (dDw/dH)/3.77 \times 10^{-15}$, we can determine dipole moments per oxygen atom of 0.54*D* for $H_0 < 0.1$ ML. If this is the case, then the Dw curve is nearly linear for $0.1 < H_0 < 1$ ML with $m = 0.12D$. This dipole moment for oxygen is the same as on Pt(111) where $m = 0.115D$ [40]. It also may be that the ''flatness'' of the Dw curve in Fig. 3 at the highest coverages, i.e. $m \cong 0$, could arise from factors other than depolarization within the adlayer such as the formation of a disordered surface (with the accompanying Au atom displacements), formation of a new chemisorbed oxygen state with a negligible dipole moment, or the incorporation of oxygen into the surface layer of gold producing no net dipole perpendicular to the surface.

3.4. X-ray photoelectron spectroscopy

The O 1s XPS spectra obtained for oxygen coverages of 0, 0.25, 0.5 and 1.0 ML are shown in Fig. 4. With increasing coverage, the O 1s peak

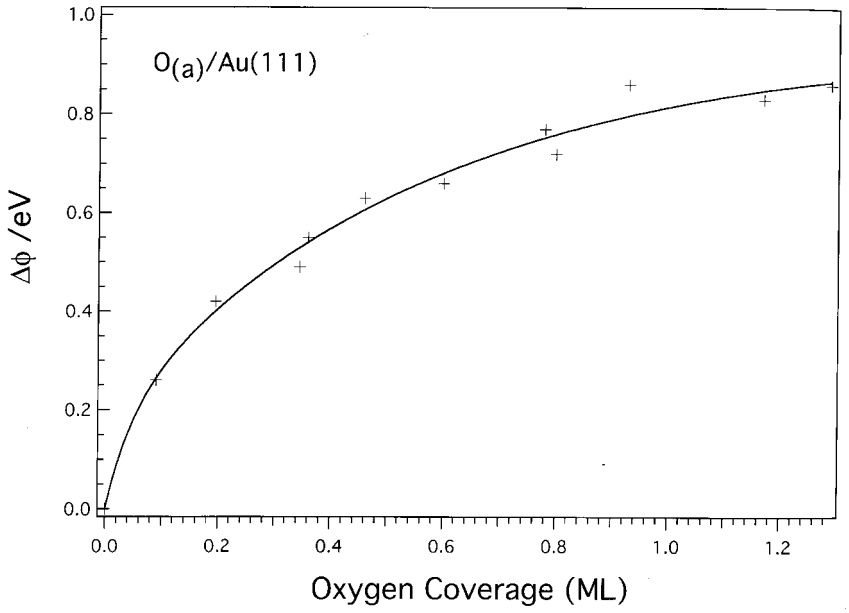

Fig. 3. Work function change Dw measured as a function of oxygen coverage. The solid curve is a fit for the data using Eq. (1).

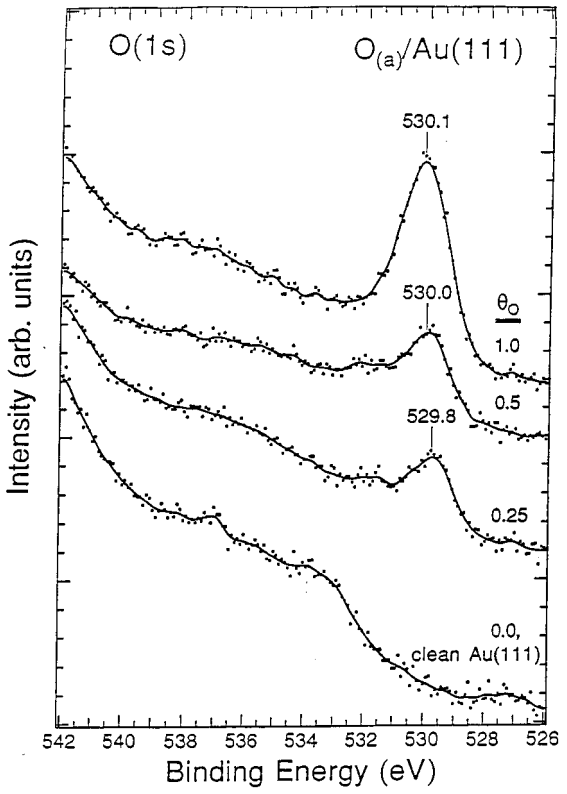

Fig. 4. O 1s XPS spectra after ozone exposure on clean Au(111) at 300 K. The oxygen coverages were determined by AES. (Taken from Ref. [29].)

undergoes a small shift from 529.8 to 530.1 eV, but the full-width-at-half-maximum stays constant at about 1.5 eV.

An O 1s peak at 530.1 eV is indicative of an ''oxidic'' chemical state for oxygen. Oxygen in an oxide is characterized by an O 1s binding energy of 530.1 eV on Au(111) [30], 530.8 eV on Ag(111) [44], 530.2 eV on Pt(111) [45], and 530.3 eV on Pd(111) [46]. Atomically adsorbed oxygen is characterized by an O 1s binding energy of 529.3 eV on Au(111) [11], 528.2 eV on Ag(111) [47], 529.8 eV on Pt(111) [48], and 529.0 eV on Pd(111) [46]. Unfortunately, XPS is not so useful in making a determination about the formation of chemisorbed O_2 under our conditions, because $O_{2(a)}$ on Pt(111) has an O 1s peak at 530.8 eV BE [49], whereas $O_{2(a)}$ on Ag(110) has an O 1s peak at 529.3 eV BE [50].

3.5. High-resolution electron energy loss spectroscopy

Vibrational spectra were obtained using HREELS following the adsorption of 1.2 ML of oxygen. The spectrum (not shown) exhibited two peaks, one at 395 cm^{-1} and a broader feature near 500 cm^{-1}. Most importantly, no other peaks were observed that would indicate the presence of molecularly adsorbed oxygen.

There is only one previous report of HREELS data for oxygen on gold, but these data indicate that all observed losses were due to SiO_2 impurities in the gold surface [26]. Regarding our spectra, we point out that the higher energy loss feature near 500 cm^{-1} was not as reproducible as the low-frequency peak, and thus it could be an artifact. The spectra were difficult to obtain in part because of the surface disorder at the higher coverages. However, previous studies on late transition metals have often identified two peaks, but both of these are generally lower than 500 cm^{-1}. For comparison, large coverages of oxygen on Ag(110) cause a peak at 339 cm^{-1} attributed to chemisorbed oxygen and a peak at 298 cm^{-1} attributed to more highly coordinated oxygen atoms [44]. Calculations by Carter and Goddard [51] suggested the presence of two nearly degenerate chemisorbed states of atomic oxygen on Ag_3 clusters, one with the form of an oxyradical anion and the other a closed-shell di-s-bonded configuration, and they calculated Ag–O stretching frequencies of 299 cm and 412 cm^{-1} for the two states, respectively. Two peaks at 330 and 403 cm^{-1} have also been observed for large oxygen coverages on Cu(110) [52]. Two Ni–O stretching frequencies were observed in $p(2\times2)$-O and $c(2\times2)$-O structures on Ni(100), and even though both vibrations result from oxygen bound in fourfold symmetric hollow sites, they differ in frequency by over 100 cm^{-1} [53].

3.6. Temperature-programmed desorption

Exposure of O_3 on Au(111) at 300 K generates an oxygen adlayer that desorbs to produce the O_2 TPD spectra shown in Fig. 5. These particular spectra were generated by increasing exposures to

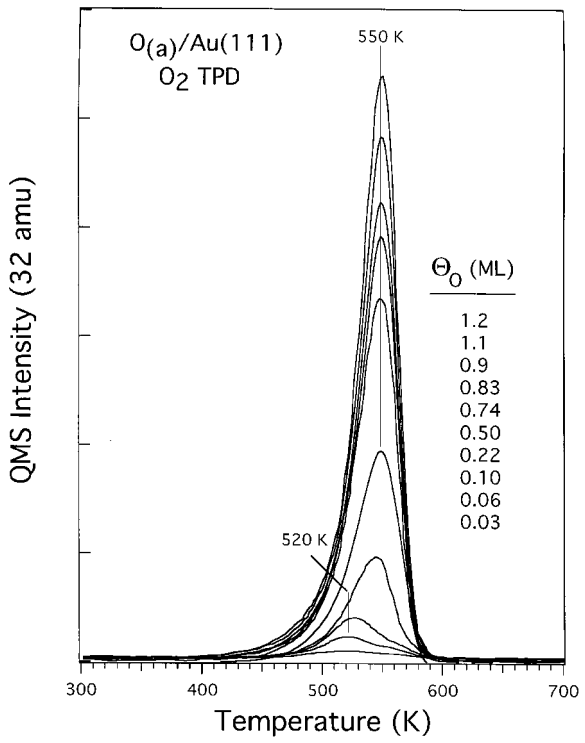

Fig. 5. Oxygen TPD following increasing exposures of ozone on Au(111) at 300 K. The oxygen coverages indicated were determined from the ratio of the integrated area under the peaks to that of the largest curve for which $H_0 = 1.2$ ML.

O_3. Identical TPD spectra could be generated in reverse by successively annealing a saturation oxygen coverage to higher temperatures. Similar exposures of O_2 to Au(111) at 300 K resulted in no detectable O_2 TPD peak. The oxygen coverages were determined by integration of the TPD peak areas, with the value for the saturation coverage calibrated by AES (vide supra).

In Fig. 5, oxygen desorption occurs initially in a peak at 520 K at the lowest oxygen coverage, and this peak shifts to higher temperatures with increasing coverages. Two of the O_2 TPD spectra at low coverage ($H_0 = 0.06$ and 0.10 ML) show features above the peak maximum that could indicate two chemical states of oxygen on the surface, with another desorption peak at about 550 K. The Au(111) reconstruction is lifted as the oxygen coverage increases up to $H_0 = 0.10$ ML, and this can be associated with the relatively large shift in the O_2 TPD peak to higher temperatures over this coverage range. The O_2 TPD peak occurs at 550 K by the time $H_0 = 0.50$ ML and does not shift with further increases in the coverage. The appearance of the peaks at high coverage offers a first hint that O_2 desorption follows first-order kinetics.

Sault et al. [27] observed similar O_2 TPD spectra from the Au(110) surface at various oxygen coverages. They assigned a region of second-order desorption kinetics at low oxygen coverages and a region of first-order kinetics at higher coverages. In addition, they attributed zero-order kinetics to the highest oxygen coverages, and they saw a shoulder on the low-temperature side of the main desorption peak. The O_2 TPD peak maximum in their work on Au(110) was at 590 K, or 40 K higher than we observed on Au(111). About 10 K of this difference is due to the difference in heating rates.

In a related system, oxygen desorption from Ag(111) [44] also closely resembles that presented above for Au(111). On Ag(111), desorption first occurs in a peak at 577 K, two O_2 TPD peaks are obtained at low coverages, at low and intermediate coverages, the peak shifts to higher temperature with increasing coverage, and at the highest coverages, the peak occurs at a constant temperature of 587 K. At high coverages, the leading edges of the desorption traces overlap as in zero-order kinetics, but the constant peak temperature indicates first-order kinetics. Using TPD, XPS, LEED, and Nuclear Reaction Analysis (NRA) on Ag(111), two different atomic states of oxygen were identified at low coverages [44]. However, a single state predominates at high coverages. This single oxygen state is attributed to the formation of an Ag_2O(111) trilayer that grows on top of the first state with a (4×4) superstructure relative to the Ag(111) substrate.

Our O_2 TPD results on Au(111) are different from those of Canning et al. [25] on the Au(111) surface. They report an O_2 desorption peak maximum at 657 K, which is over 100 K higher than we observe. This difference could be due to incorrect temperature readings in their experiments since their thermocouple was attached to a tantalum sample holder held in contact with the crystal

(in our experiments, the thermocouple was mounted directly in the crystal), and their ramp rate was 21.5 K s^{-1} (almost three times higher than ours), or possibly (but less likely) to the high degree of surface disorder reported by Canning et al. [25]. The calibration of our Au(111) crystal temperature was checked by performing thermal desorption of a water multilayer. We found that the H_2O heat of sublimation of 12 kcal mol^{-1} was in good agreement with previously reported values for Ni [54], Ir [55], and Pt [56].

Redhead analysis [57] gives desorption activation energies, E_d, of 31.7–33.6 kcal mol^{-1} over the full coverage range assuming a pre-exponential factor for desorption n_d of 1×10^{13} s^{-1} and first-order kinetics. We have employed two different analysis methods in order to obtain better estimates for the kinetic parameters describing the O_2 desorption process. First, we used an analysis method that allowed for the determination of the reaction order [40,58], involving plotting $[\ln(dH/dt)-n\ln(H)]$ versus $(1/T)$ for the entire temperature range of the desorption data. This plot is only linear for the correct choice of n, and the slope of the plot gives E_d. Secondly, as a check on the validity of the kinetic parameters obtained from this method, we have compared computer simulations of the desorption rate curves with the experimental TPD data.

The TPD spectra at high coverages in Fig. 5 have an appearance that is indicative of first-order kinetics even though the recombination of O adatoms to form O_2 is expected to be a second-order process. In order to determine the reaction order for desorption, we made plots of $[\ln(dH/dt)-n\ln(H)]$ versus $(1/T)$ for each of the spectra shown in Fig. 5. Fig. 6 shows one example of a plot for the case $H_0=0.22$ ML. As can be seen, the best fit to a line was obtained when n was chosen to be 1. Also, the other choices of n gave the predicted curves [58] for incorrect choices of the reaction order. The intercept of the line shown in Fig. 6 gives a value of 2.7×10^{11} s^{-1} for the pre-exponential factor for desorption, and the slope gives a value of $E_d=28.6$ kcal mol^{-1}. For $H_0=0.03$ ML, $n_d=5.5\times10^{11}$ s^{-1} and $E_d=23.2$ kcal mol^{-1}. The plots obtained in this manner for higher coverages are also best described with $n=1$, but show some curvature. In each case, these plots have a linear region with a lower slope ($n_d=8.2\times10^{9}$–

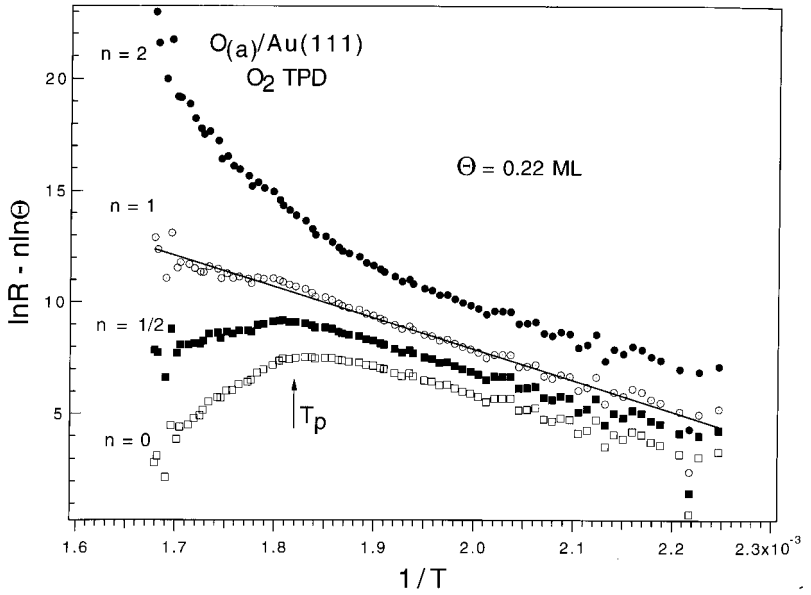

Fig. 6. Oxygen TPD curves for $H_0=0.22$ ML plotted using the method of Parker et al. [58]. Plots for several choices of n, the desorption kinetic order, are shown, and only the data for $n=1$ can be described well by a line in the region of T_p.

10×10^{10} s^{-1} and $E_d = 23$–25 kcal mol^{-1}) for $\Theta_O > 0.5$ ML and $T > 520$ K, and another region with a higher slope with values of $n_d = 7.8 \times 10^{10}$–3.8×10^{11} s^{-1} and $E_d = 26.7$–30 kcal mol^{-1}. In summary, we find that E_d increases with coverage. At low coverages, $E_d = 23.2$ kcal mol^{-1} at $\Theta_O = 0.03$ ML and 28.6 kcal mol^{-1} at $\Theta_O = 0.22$ ML. E_d then shows a very slight increase to 30 kcal mol^{-1} near saturation coverages. The curvature of some of the plots indicates that at high coverages, there is a second oxygen state that desorbs with a lower E_d of 23–25 kcal mol^{-1}.

Simulations of the TPD spectra for $\Theta_O = 0$–1.2 ML are directly compared to the measured spectra in Fig. 7. The simulations used a Polanyi–Wigner desorption rate equation using a coverage-dependent activation energy of the form

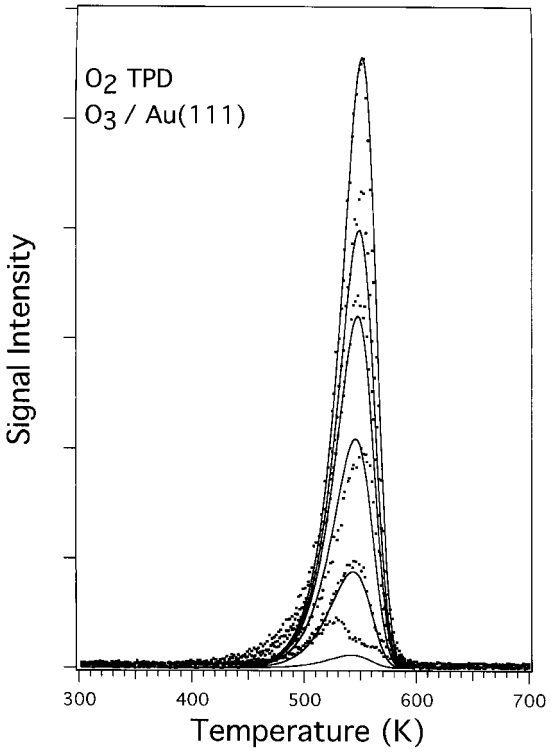

Fig. 7. Computer simulation (solid curve) of the TPD data (points) in Fig. 5. This simulation used a Polanyi–Wigner form of the desorption rate equation with first-order kinetics, a value of 5.5×10^{11} s^{-1} for the pre-exponential factor, and a coverage-dependent activation energy of $E_d = 30 + 0.75(\Theta_O/\Theta_{O_{max}})$ (kcal mol^{-1}), with $\Theta_{O_{max}} = 1.2$ ML.

$E_d = 30 + 0.75(\Theta_O/\Theta_{O_{max}})$, where $\Theta_{O_{max}} = 1.2$, with a constant pre-exponential factor of 5.5×10^{11} s^{-1}. The small linear coverage dependence was necessary to produce peaks with the best fit for the width and shape. This simulation gives a good fit to the experimental data and shows that the values for the kinetic parameters derived from our data analysis above are quite reasonable.

One noticeable feature of Fig. 7 is the poor fit of the simulations to the leading edge of the desorption curves. The measured desorption rate is much higher than that predicted by the simulations, consistent with a lower value for E_d at the highest coverages (lowest temperatures) for each of the curves for $\Theta_O \geq 0.5$ ML. No choices of a single coverage-dependent activation energy or wide-ranging values of n_d could give a fit over this leading edge region as well as the main peak. We are forced to conclude that another desorption state is present that has a lower E_d of 23–25 kcal mol^{-1} at high coverages, but that this state is not resolved from the main peak in our experiments. This is consistent with the curvature and slopes observed in the plots like that in Fig. 6. As pointed out above, Sault et al. [27] observed a shoulder on the low-temperature side of the main O_2 desorption peak on Au(110), and so a small energy change in the two peaks could cause them to desorb more nearly at the same temperature.

From the value for E_d obtained from the TPD analysis, we now estimate the O–Au bond strength. In the simplest interpretation, the measured value of 30 kcal mol^{-1} at $\Theta_O = 1.2$ ML reflects the activation energy for desorption from the dissociative adsorbed state, which is the sum of the adsorption energy or enthalpy, ΔH_a, of dissociative adsorption of O_2 on Au(111), and the activation barrier to dissociative adsorption of O_2, E_a. We know that O_2 adsorption is activated since the surface cannot be populated with O adatoms from exposure in UHV to O_2. Since $E_d = E_a + \Delta H_a$, 30 kcal mol^{-1} is an upper limit for ΔH_a since $E_a > 0$. The bond dissociation energy of D(Au–O) is given by:

$$2D(\text{Au–O}) = D(\text{O–O}) + \Delta H_a. \quad (2)$$

The bond strength in dioxygen is D(O–O) = 119 kcal mol^{-1}, and so since $\Delta H_a \leq 30$ kcal mol^{-1}, D(Au–O) ≤ 74.5 kcal mol^{-1}. Å much

better estimate for the true value of the Au–O bond strength can be made by utilizing reports in the literature to estimate a value for E_a. For example, the data of Ref. [27], in which no oxygen adsorption occurred on Au(110)-(1×2) for exposures at $P_{O_2}=1400$ Torr for 10 min on Au(111) at 900 K leads to an estimation of $E_a \geq 37$ kcal mol^{-1} by assuming a detection sensitivity of 0.01 ML and a precursor-mediated dissociation mechanism in which a preequilibrium is established with molecularly adsorbed O_2 having an adsorption energy of 5 kcal mol^{-1} (the barrier for dissociation from this state is calculated to be ≥ 42 kcal mol^{-1}). The value of 5 kcal mol^{-1} in this calculation was estimated from the observation that no molecular O_2 desorption peak has been observed above 100 K (and assuming that no substantial barrier exists between the physisorbed and chemisorbed molecular state $E_1 \approx 3$ kcal mol^{-1} [47]). One can consider the adsorption energy for chemisorbed O_2 on Ag(111) as an upper limit at 9.2 kcal mol^{-1} [47] and physisorbed O_2 on Ag(111) as a lower limit at 3 kcal mol^{-1} [47]. Another, but less reliable, value of $E_a \sim 15$ kcal mol^{-1} can also be estimated by utilizing data for oxygen adsorption on (Ag–Au)/a-Al_2O_3 catalysts [59] and extrapolating their E_a curve for varying Au composition to the limit of pure Au. A value of $E_a = 37$ kcal mol^{-1} gives a value for DH_a that is 7 kcal mol^{-1} (endothermic) and thus D(Au–O)$\sim$56 kcal mol^{-1}. This estimate can be compared to D(Au–Cl)=54 kcal mol^{-1} [60], D(Ag–O)=80 kcal mol^{-1} on Ag(111) [47], D(Pt–O)=85 kcal mol^{-1} in the limit of zero coverage on Pt(111) [39], and an estimate of D(Pt–O)$\sim$65 kcal mol^{-1} for $H_0 = 0.75$ ML on Pt(111) [40]. Fig. 8 shows our best estimates for a potential energy diagram for oxygen adsorption on Au(111). This diagram shows gaseous, adsorbed and oxidic states of oxygen that are useful for discussing the oxygen/Au interaction. We show the heat of formation of Au_2O_3(s) as a rough indicator of the energetics of oxidic species that may be formed. The adsorption energy of physisorbed and chemisorbed O_2 is taken to be 3 kcal mol^{-1}, and the barrier between physisorbed and chemisorbed O_2 is taken to be 3 kcal mol^{-1}, as on Ag(111) [47]. E_2 is the barrier for dissociation from an accommodated chemisorbed O_2 species.

The first-order kinetics of the O_2 desorption peaks from Au(111) is not easily explained. Molecular desorption of atomically adsorbed species is generally found to occur with second-order kinetics. Our results indicate that the recombination of atomic oxygen is not the rate-limiting

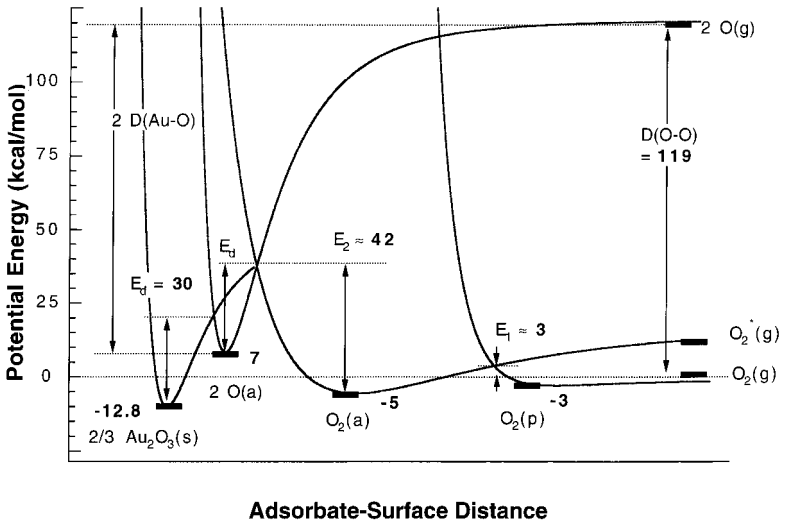

Fig. 8. Schematic potential energy diagram of the oxygen interaction with Au(111). Values for the heats of formation of gaseous, adsorbed and oxidic species are indicated by solid bars.

step in the desorption process, and so this complicates the analysis and energetics discussed above. We propose that the rate-limiting step for desorption is the conversion of an oxidic oxygen species to chemisorbed oxygen, and this explanation is consistent with recent XPS studies of UV/ozone oxidation of Au [30]. In Fig. 8, the formation energy of Au_2O_3 is only slightly exothermic, and the conclusion that a kinetic barrier of 30 kcal mol^{-1} for conversion of the oxide to adsorbed oxygen is larger than the barrier for conversion of O adatoms to chemisorbed O_2 is plausible. Since the Au surface is highly disordered at high coverages, it is also possible that the rate-limiting step for O_2 desorption involves the displacement of a gold atom leading to first-order kinetics [61] rather than oxide conversion. If a surface ''compound'' (Au_2O_3) is formed, we could also be simply observing a first-order decomposition step. Finally, O_2 desorption might be rate-limited by the formation of a molecularly chemisorbed precursor state having first-order desorption kinetics, but would then imply an anomolously large barrier of 24 kcal mol^{-1} between the physisorbed and chemisorbed molecular species, and there is no spectroscopic evidence to suggest that a molecularly chemisorbed precursor exists on the surface.

4. Summary

Moderate exposures of ozone to the Au(111) surface at room temperature under UHV conditions generate oxygen concentrations up to 1.2 ML. No molecularly adsorbed O_2 state was detected by HREELS, but XPS was not definitive for identification of oxidic species in addition to chemisorbed oxygen adatoms. Incorporation of oxygen to form a surface oxide at high coverages is indicated by several results. No ordered superlattice for the oxygen overlayer was observed, and disordering of the Au(111) substrate occured at higher coverages. A $D\Phi$ value of $+0.76$ eV and a dipole moment of 0.12*D* for oxygen on Au (111) at $\theta_O = 0.75$ ML are about the same as those for atomic oxygen on Pt(111). A clean surface can be regenerated by heating the oxygen-covered Au(111) surface to 600 K due to the thermal desorption of O_2. First-order kinetics describes O_2 desorption, and this process is probably rate-limited by conversion of oxidic oxygen to chemisorbed atomic oxygen. Analysis of the TPD data indicates a rapidly increasing O_2 desorption activation energy from 23.2 to 28.6 kcal mol^{-1} at low coverages, followed by a very slightly increasing activation energy up to 30 kcal mol^{-1} near saturation coverage. From our TPD data and a reasonable estimate for the activation barrier to O_2 dissociative adsorption, we estimate an upper limit on the O–Au bond strength to be 64 kcal mol^{-1}.

Acknowledgements

Acknowledgment is made to the Donors of the Petroleum Research Fund, administered by the American Chemical Society, for partial support of this work. The authors would like to thank Alan Hills at the University of Colorado, Boulder for his assistance in our first attempts to prepare ozone. We would also like to thank Dr. Michel Van Hove for helpful discussions, and Dave Wickham and Dr. Mark Jones for their work in developing the computer programs for the TPD simulations and data analysis.

References

[1] B. Hammer, J.K. Norskov, Nature 376 (1995) 238.
[2] J. Schwank, Gold Bull. 16 (1983) 103.
[3] M. Haruta, T. Kobayashi, H. Sano, N. Yamada, Chem. Lett. 2 (1987) 405.
[4] M. Haruta, T. Kobayashi, S. Iijima, F. Delannay, in: Proceedings of the Ninth International Congress on Catalysis, vol. 3, 1988, p. 1206.
[5] M. Haruta,, H. Kageyama, N. Kamijo, T. Kobayashi, F. Delannay, in: T. Innui (Ed.), Successful Design of Catalysts, Elsevier, Amesterdam, 1988, p. 33.
[6] M. Haruta, K. Saika, T. Kobayashi, S. Tsubota, Y. Nakahara, Chem. Express 3 (1988) 159.
[7] M. Haruta, N. Yamada, T. Kobayashi, S. Iijima, J. Catal. 115 (1989) 301.
[8] S. Tsubota, N. Yamada, M. Haruta, T. Kobayashi, Y. Nakahara, Chem. Express 5 (1990) 349.
[9] S. Tsubota, M. Haruta, T. Kobayashi, A. Ueda, Y. Nakahara, in: G. Poncelet, P.A. Jacobs, P. Grange, B.

Delmon (Eds.), Preparation of Catalysts, vol. V, Elsevier, Amsterdam, 1991, p. 695.
[10] S.D. Gardner, G.B. Hoflund, B.T. Upchurch, D.R. Schryder, E.J. Kielin, J. Schryder, J. Catal. 129 (1991) 114.
[11] S. Takamatsu, M. Ishi-i, M. Imagawa, H. Kinbara, T. Kibuta, T. Fukushima, Catal. Soc. Jpn. 34 (1992) 126.
[12] A. Knell, P. Barnickel, A. Baiker, W. Wokaum, J. Catal. 137 (1992) 306.
[13] M. Haruta, S. Tsubota, T. Kobayashi, H. Kageyama, M.J. Genet, B. Delmon, J. Catal. 144 (1993) 175.
[14] D. Cunningham, S. Tsubota, N. Kamijo, M. Haruta, Res. Chem. Intermed. 19 (1993) 1.
[15] S.D. Lin, M. Bollinger, M.A. Vannice, Catal. Lett. 17 (1993) 245.
[16] C. Sze, E. Gulari, B. Demczyk, Mater. Res. Soc. Symp. Proc. 286 (1993) 143.
[17] S.K. Tanielyan, R.L. Augustine, Appl. Catal. A 85 (1992) 73.
[18] M.A. Bollinger, M.A. Vannice, Appl. Catal. B 8 (1996) 417.
[19] Z.M. Liu, M.A. Vannice, Catal. Lett. 43 (1997) 51.
[20] M.A. Chesters, G.A. Somorjai, Surf. Sci. 52 (1975) 21.
[21] M.E. Schrader, Surf. Sci. 78 (1978) L227.
[22] D.D. Eley, P.B. Moore, Surf. Sci. 76 (1978) L599.
[23] P. Legaré, L. Hilaire, M. Sotto, G. Maire, Surf. Sci. 91 (1980) 175.
[24] J.J. Pireaux, M. Chtaïb, J.P. Delrue, P.A. Thiry, M. Liehr, R. Caudano, Surf. Sci. 141 (1984) 211.
[25] N.D.S. Canning, D. Outka, R.J. Madix, Surf. Sci. 141 (1984) 240.
[26] J.J. Pireaux, M. Liehr, P.A. Thiry, J.P. Delrue, R. Caudano, Surf. Sci. 141 (1984) 221.
[27] A.G. Sault, R.J. Madix, Surf. Sci. 169 (1986) 347.
[28] D.H. Parker, B.E. Koel, J. Vac. Sci. Technol. A 8 (1990) 2585.
[29] M.A. Lazaga, D.T. Wickham, D.H. Parker, G.N. Kastanas, B.E. Koel, in: J.W. Hightower, S.T. Oyama (Eds.), Catalytic Selective Oxidation, ACS Symposium Series, ACS, Washington, DC, 1993, p. 90.
[30] A. Krozer, M. Rodah, J. Vac. Sci. Technol. A 15 (1997) 1704.
[31] D.E. King, J. Vac. Sci. Technol. A 13 (1995) 1247.
[32] F. Cotton, G. Wilkinson, Inorganic Chemistry, 3rd ed., Wiley, New York, 1972, p. 994.
[33] J. Cao, N. Wu, S. Qi, K. Feng, M.S. Zei, Chinese Phys. Lett. 6 (1989) 92.
[34] J. Chevrier, L. Huang, P. Zeppenfeld, G. Comsa, Surf. Sci. 355 (1996) 1.
[35] L. Huang, P. Zeppenfeld, J. Chevrier, G. Comsa, Surf. Sci. 352–354 (1996) 285.
[36] L. Huang, J. Chevrier, P. Zeppenfeld, G. Comsa, Appl. Phys. Lett. 66 (1995) 935.
[37] R.G. Windham, M.E. Bartram, B.E. Koel, J. Phys. Chem. 92 (1988) 2862.
[38] R.J. Koestner, Ph.D. thesis, University of California, Berkeley, CA, publication no. LBL-14766.
[39] D.M. Zehner, J.F. Wendelken, Proc. 7th Int. Vac. Congr. 3rd Int. Conf. Solid Surfaces, Vienna, 1977, p. 517.
[40] D.H. Parker, M.E. Bartram, B.E. Koel, Surf. Sci. 217 (1989) 489.
[41] Handbook of Auger Electron Spectroscopy, 2nd ed., Perkin-Elmer, Eden Prairie, MN, 1976.
[42] J.R. MacDonald, C.A. Barlow, Jr, J. Chem. Phys. 39 (1963) 412.
[43] J.R. MacDonald, C.A. Barlow, Jr, J. Chem. Phys. 44 (1966) 202.
[44] S.R. Bare, K. Griffiths, W.N. Lennard, H.T. Tang, Surf. Sci. 342 (1995) 185.
[45] M. Peuckert, H.P. Bonzel, Surf. Sci. 145 (1984) 239.
[46] B.A. Banse, B.E. Koel, Surf. Sci. 232 (1990) 275.
[47] C.T. Campbell, Surf. Sci. 157 (1985) 43.
[48] G.B. Fisher, J.L. Gland, Surf. Sci. 94 (1980) 446.
[49] G.B. Fisher, B.A. Sexton, J.L. Gland, J. Vac. Sci. Technol. 17 (1980) 144.
[50] C.T. Campbell, M.T. Paffett, Surf. Sci. 143 (1984) 517.
[51] E.A. Carter, W.A. Goddard, Surf. Sci. 209 (1989) 243.
[52] A.P. Baddorf, J.F. Wendelken, Surf. Sci. 256 (1991) 264.
[53] S. Andersson, Surf. Sci. 79 (1979) 385.
[54] R.H. Stulen, P.A. Thiel, Surf. Sci. 157 (1985) 99.
[55] T.S. Wittrig, D.E. Ibbotson, W.H. Weinberg, Surf. Sci. 120 (1981) 506.
[56] G.B. Fisher, J.L. Gland, Surf. Sci. 94 (1980) 446.
[57] P.A. Redhead, Vacuum 12 (1962) 203.
[58] D.H. Parker, M.E. Jones, B.E. Koel, Surf. Sci. 233 (1990) 65.
[59] D.I. Kondarides, X.E. Verykios, J. Catal. 158 (1996) 363.
[60] G.N. Kastanas, B.E. Koel, Appl. Surf. Sci. 64 (1993) 235.
[61] V.P. Zhdanov, J. Phys. Chem. 93 (1989) 5582.